Acta Geochim (2021) 40(3):300–311
https://doi.org/10.1007/s11631-021-00453-7

ORIGINAL ARTICLE

Interaction of Ca^{2+} and soil humic acid characterized by a joint experimental platform of potentiometric titration, UV–visible spectroscopy, and fluorescence spectroscopy

Haiming Tang[1,2] · Baohua Xiao[1] · Peiwen Xiao[1,2]

Received: 29 October 2020 / Revised: 16 December 2020 / Accepted: 12 January 2021 / Published online: 26 January 2021

Abstract Rocky desertification has become a major environmental issue in the karst region of southwestern China. Karst rocky desertification was more severe in regions of limestone soil than in adjacent regions of other soils, despite the relatively higher soil organic matter (SOM) content in limestone soil. The underlying mechanism remains ambiguous. We speculated that the geochemical characteristics of limestone soils in the karst region plays an essential role, especially the high calcium content of limestone soil. To test this hypothesis, we collected limestone soil samples from a limestone soil profile in the southwestern China karst region and extracted humic acid (HA) from these limestone soil samples. We investigated the interaction of Ca^{2+} and three HA samples on a joint experimental platform, which consists of an automatic potentiometric titrator, a UV–visible spectrometer, and a Fluorescence spectrometer. HA solutions were titrated by Ca^{2+} and optical spectra of the HA solutions were monitored during the titration experiments. The results indicated that: (1) the interaction of Ca^{2+} and HA is a combined process of adsorption and complexation. Adsorption dominated the overall distribution behavior of Ca^{2+}, which could be fit by Langmuir and Freundlich isotherm models. Complexation was distinguished only when the concentration of Ca^{2+} is low; (2) the changes of UV–visible spectroscopy and excitation–emission matrix fluorescence spectroscopy spectra of HA samples when they were binding with Ca^{2+} implied the apparent molecular size and structure of HA became larger and more complex; (3) the combination of Ca^{2+} and HA plays an important role in the SOM preservation of limestone soils but the stability of the Ca–HA association was relatively weak. The present study draws attention to maintaining the relatively higher Ca^{2+} concentration in limestone soils in ecologic restoration attempts in karst regions.

Keywords Limestone soil · Humic acid · Calcium · Interaction · Titration · UV–Vis · EEM

1 Introduction

The karst landscape is a typical natural landscape accounting for approximately 12% of the world's total terrestrial area (Derek and Paul 2007; Liu 2009). The karst region in southwestern China is the largest karst region with continuous carbonate rock outcrops. This region suffers a series of environmental problems, especially, the karst rocky desertification, due to the rapid population growth and economic development over the last two decades (Wang 2003; Wang et al. 2004; Liu 2009). Different karst rocky desertification situations had been observed (Bai et al. 2011) and limestone soil regions often found more severe karst rocky desertification situations compared to adjacent regions of other soils in the southwest China karst region (Zheng and Wang 2002; Yan et al. 2019) despite the relatively higher SOM content in limestone soils (Liu 2009; Di et al. 2019). Yet what role the characteristics of soil plays during the occurrence of karst rocky desertification is largely unknown.

✉ Baohua Xiao
xiaobaohua@mail.gyig.ac.cn

[1] State Key Laboratory of Environmental Geochemistry, Institute of Geochemistry Chinese Academy of Sciences, Guiyang 550081, Guizhou, China

[2] University of Chinese Academy of Sciences, Beijing 100049, China

Soil organic matter (SOM) is an important component of soil and contributes the most to the properties and service functions of soil (Osman 2013; Coleman and Wall 2014). SOM is the largest reactive carbon pool, and its turnover kinetics has the compound feedbacks to the climate changes (Schmidt et al. 2011). Several potential mechanisms of SOM stabilization in the soil had been proposed, for example, the inherent recalcitrance or thermodynamic stability of SOM, the selective preservation of SOM by decomposers, the physical occlusion between SOM and decomposers, and the sorption of SOM by soil minerals to form organo-mineral complexes (Sollins et al. 1996). However, recent studies argued that the SOM stabilization in soil was mainly driven by ecosystem properties rather than the different inherent recalcitrance of SOM fractions (Schmidt et al. 2011; Lehmann and Kleber 2015). The mechanisms of SOM protection are still controversial and demand more extensive studies.

Humic substances, the major fraction of SOM, are complex mixtures of natural organic macromolecules produced by biotic and abiotic transformations of plant, microbial, and animal residues in soil (Aiken et al. 1985). Because of the high complexity and heterogeneity, humic substances are often divided into three principal fractions, that is, humic acids (HA), fulvic acids (FA), and humin (HM) (Stevenson 1994). Of the three, HA is moderate in terms of either biochemical stability or biochemical activity and is viewed as the principal structural humic substances in soil (Stevenson 1994; Jones and Bryan 1998; Agnelli et al. 2002; Janoš et al. 2008). Characterization studies on HA help to understand the composition and evolution of SOM, which are of great significance in the reasonable utilization and remediation of soil resources (Piccolo and Mbagwu 1994; Osman 2013). The SOM stabilization studies were mainly focused on interactions between SOM and iron-aluminum oxides in acidic soils (Grünewald et al. 2006; Kogelknabner et al. 2008; Gerke 2010; Zhao et al. 2017), but few studies on neutral to alkaline soils were reported. Limestone soil, which usually forms on the carbonate rocks, is a typical neutral to alkaline soil with a relatively high content of Ca^{2+} and SOM (Baldock and Skjemstad 2000; Bollag and Stotsky 2000; Liu 2009; Kloster et al. 2013), and its physicochemical properties are much different from those of other soils in the karst region (Di et al. 2019; Yan et al. 2019). Many studies had speculated that HA could complex with Ca^{2+} to form stable humic-Ca complexes (Duchaufour 1976; Oades 1988; Begum et al. 2018), and the humic-Ca complexes might influence the accumulation and transformation of SOM in the limestone soil (Ma et al. 2016; Di et al. 2019). However, systematical and quantitative studies on the interaction between Ca^{2+} and HA from limestone soils were seldom reported, and whether $CaCO_3$ or Ca^{2+} effects characteristics of HA is still controversial (Jin and Zimmerman 2010; Plank and Bassioni 2007; Begum et al. 2018; Jin et al. 2018).

The primary objective of this study is to investigate interactions between Ca^{2+} and HAs isolated from limestone soils in the aqueous solution and to characterize changes of the apparent molecular properties of HA in the solution as the coexisting Ca^{2+} concentration increasing. For this purpose, we designed a joint continuous experimental system comprised of a potentiometric titrator, UV–visible spectroscopy (UV–Vis), and fluorescence spectroscopy as the main experimental platform. The potentiometric titration, UV–Vis, and excitation–emission matrix (EEM) fluorescence spectroscopy spectra had been used widely in many kinds of research and each of them had obtained instructive results. Usually, these techniques were applied separately (Abate and Masini 2001; Chen et al. 2002; He et al. 2016), and data from different studies lacked consistency. We here tried to combine these three techniques into a measurement platform so that we can monitor in real-time the free concentration of Ca^{2+} in HA solution during the titration and observe UV–Vis and EEM fluorescence spectra of the HA solution simultaneously. The systematic study of the interaction between HA and Ca^{2+} can improve understandings of how Ca^{2+} influences the stability of SOM in the limestone soil of karst regions and provide theoretical supports for strategies of mitigating karst rocky desertification.

2 Materials and methods

2.1 Preparation and characterization of soil and soil HA samples

The limestone soils used in this study are the typical soil of the southwest karst region of China. The limestone soils were collected from a limestone soil profile (25.307° N, 107.936° E) in the Maolan Natural Karst Forest reserve, Guizhou, China, where the annual average temperature is 18 °C and the annual precipitation is 765 mm. Before sampling, the surface of the site was cleaned for plant litter removal. A total of three soil samples were taken from an area of 50 cm by 50 cm at three layers with depths of 0–12 cm (L1), 12–24 cm (L2), and 24–36 cm (L3). According to the field observation, the sampling interval was determined that the soil color shifted slightly at a depth of 12 cm. The soil samples were air-dried and slightly crashed to pass the sieve of 2 mm, and visible debris of rock and plant was manually picked out. The pH of the three limestone soils (L1, L2 and L3) are 6.4, 6.3, and 6.3, respectively (measured at the soil:H_2O ratio of 1:5). The HA samples were obtained by extracting the three soil

samples with NaOH solution (0.5 mol/L), the extraction operations were detailed elsewhere (Ma et al. 2016). HA samples were labeled according to the collecting depth of soil samples: L1HA (0–12 cm), L2HA (12–24 cm), L3HA (24–36 cm). The elemental compositions and primary physicochemical properties of three limestone soils and three HA samples were list in Table 1, and the distribution of functional groups in three HA samples (measured by ^{13}C-NMR) was described in Table 2.

2.2 Mensuration of the interaction between Ca^{2+} and HA

An exact amount of a HA sample (10.0 mg) was carefully dissolved in 100 mL NaCl solution (0.1 mol/L) which was purged previously by N_2 gas and shook mildly under N_2 gas protection for 12 h to obtain the initial HA solution. The concentration and ionic strength of the initial HA solution were 100 mg/L and 0.1 M, respectively. Then, the exact volume of the initial HA solution (40 mL) was transferred into a titration cup (100 mL) for the following experiments. The joint experimental platform comprised three experimental units, an automatic potentiometric titrator (Mettler Toledo T50), a UV–visible spectrometer (Agilent Cary 300), and a fluorescence spectrometer (Hitachi F-4500), and the three experimental units were sequentially connected by several Tygon tubes so that the HA solution can be circulated in the system by a peristaltic pump (Millipore). All measurements were conducted under 25 °C with the N_2 gas protection after the HA solution flow became stable. In the automatic potentiometric titration experiment, the HA solution was titrated by the $CaCl_2$ solution (1 mol/L) with an increment of 0.02 mL and a titration interval of 120 s until the total concentration of Ca^{2+} in the solution reached 0.07 mol/L, the real-time concentration of free Ca^{2+} ion in the solution was measured by a Ca^{2+}-ISE electrode (Mettler Toledo perfectION^{TM}) during the potentiometric titration. In the meantime, the UV–Vis and the EEM fluorescence spectra of the HA solution were monitored at predetermined times. The UV–Vis spectrometer was set to scan the wavelength range of 800–200 nm at the scanning rate of 600 nm/min. The EEM fluorescence spectroscopy was set to scan the excitation range of 240–450 nm and the emission range of 300–510 nm at the same scanning rate of 2400 nm/min. 5 pairs of UV–Vis and EEM spectra were obtained for each HA solution when the total concentration of Ca^{2+} in the solution was 0.00, 0.002, 0.004, 0.01, and 0.07 mol/L, respectively.

Table 1 The basic properties of soil and soil HA samples

Characteristics of limestone soil								
Soil	pH	Organic element (wt%)			Mineral (wt%)			
		TOC	TON	TOS	SiO_2	Al_2O_3	Fe_2O_3	CaO
L1	6.44	3.12	0.34	0.62	59.10	14.16	6.00	2.16
L2	6.25	2.26	0.25	0.45	60.30	14.41	5.81	2.25
L3	6.34	1.92	0.22	0.43	61.56	14.65	6.21	2.37

Characteristics of HA in limestone soil								
HA	Organic element (wt%)				Atomic ratio (%)			Ash (wt%)
	C	H	O	N	C/N	H/C	O/C	
L1HA	49.52	5.72	38.68	6.53	8.85	1.39	0.59	3.42
L2HA	48.73	5.41	40.82	5.64	10.08	1.33	0.63	1.83
L3HA	47.36	4.83	42.27	5.50	10.05	1.22	0.67	1.42

2.3 Data collection and analysis

2.3.1 Potentiometric titration

The free Ca^{2+} concentration in the HA solution was measured directly by the potentiometric titrator equipped with a Ca^{2+}-ISE electrode, the concentration Ca^{2+} bound with HA was calculated by the mass balance equation (1),

$$q_e = V \times \frac{(C_t - C_e)}{M} \quad (1)$$

where q_e is the concentration of Ca^{2+} bound with HA (mol/kg), V is the volume of the HA solution (l), M is the weight of the HA sample (kg), C_t and C_e are the calculated total concentration of Ca^{2+} in the solution and the concentration of free Ca^{2+} in the HA solution measured by the Ca^{2+}-ISE (mol/L), respectively. The Langmuir model, the Freundlich model, the Langmuir–Freundlich model and the Toth model were employed to fit the titration experimental data to investigate underlying binding processes of Ca^{2+} on HA. The Langmuir model, the Freundlich model, the Langmuir–Freundlich model, and the Toth model are described by Eqs. (2), (3), (4), and (5), respectively:

$$\text{Langmuir model: } q_e = \frac{Q_m \times b \times C_e}{1 + b \times C_e} \quad (2)$$

$$\text{Freundlich model: } q_e = K_F \times C_e^n \quad (3)$$

$$\text{Langmuir}-\text{Freundlich model: } q_e = \frac{Q_m \times (b \times C_e)^n}{1 + (b \times C_e)^n} \quad (4)$$

$$\text{Toth model: } q_e = \frac{Q_m \times (b \times C_e)^n}{\left[1 + (b \times C_e)^n\right]^{1/n}} \quad (5)$$

where for all equations, C_e is the concentration of free Ca^{2+} in the HA solution (mol/L) and q_e is the concentration of Ca^{2+} bound with HA (mol/kg); Q_m is the maximum

Table 2 The functional groups distribution in three HA samples (calculated from ^{13}C-NMR spectra)

Chemical shift (ppm) Functional groups	0–45 Alkyl group	45–60 Methoxy group	60–110 Carbo-hydrate	110–140 Aromatic group	140–160 Phenolic group	160–185 Carboxyl group	185–230 Ketonic group
L1HA	15.63	7.98	30.84	19.65	10.29	10.28	5.34
L2HA	14.66	7.91	29.40	21.75	10.99	10.38	4.92
L3HA	17.31	9.52	35.60	19.37	8.01	6.88	3.32

concentration of Ca^{2+} can be sorbed by HA (mol/kg) and b is the model parameter related to the sorption energy (l/mol) in Eqs. (2), (4) and (5); n is the model parameter related to the heterogeneity of available sorption sites in Eqs. (3), (4) and (5); K_F in Eq. (3) is the Freundlich parameter related to the sorption capacity. The titration results of the three HA samples and the fit curves by different sorption models were plotted in Fig. 1.

2.3.2 *UV–visible spectroscopy*

A series of optical parameters calculated from the UV–Vis spectrum of HA had been suggested to quantify the physicochemical characteristics of HA (Chen et al. 1977; Helms et al. 2008; Vidal et al. 2016). In this study, we selected three optical parameters, E_4/E_6, E_2/E_3, and $\Delta \log K$, to investigate changes of the apparent molecular size,

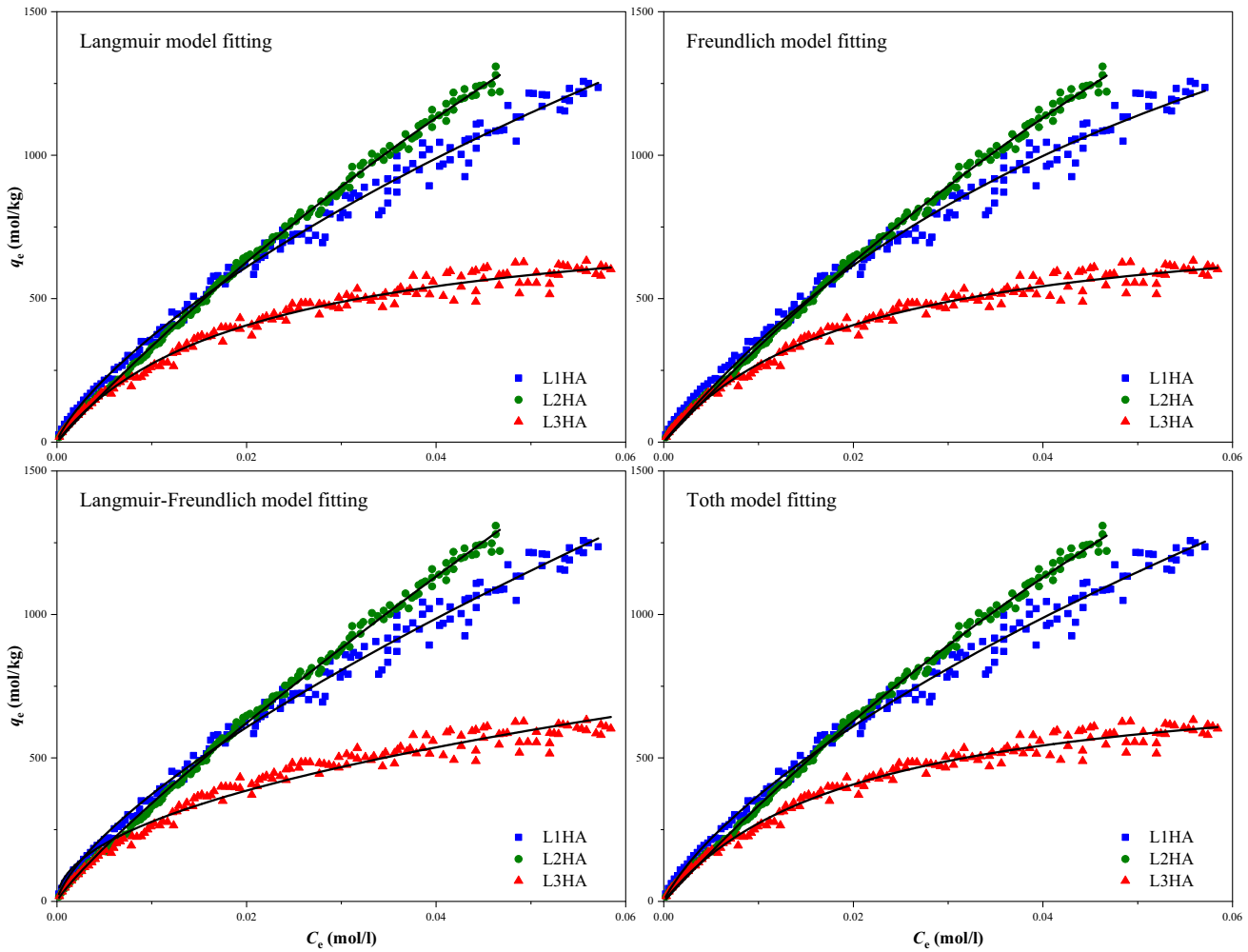

Fig. 1 The HA-bound Ca^{2+} concentration in HA samples *Vs* the free Ca^{2+} concentration in the solutions during titration experiments and their sorption models fitting curves. *Note*: C_e (mol/L) is the equilibrium free Ca^{2+} concentration in the solution; q_e (mol/kg) is the equilibrium HA-bound Ca^{2+} concentration in HA samples

weight, and structural complexity for the HA sample during its interaction with different concentrations of Ca^{2+}. Briefly, the E_4/E_6 value, one of the most used parameters in SOM characterization studies, refers to the ratio of absorbances at 465 nm and 665 nm in the UV–Vis spectrum. Prior studies had shown that the E_4/E_6 value was a good indicator for the molecular weight of HA, the lower the E_4/E_6 value, the heavier the molecular weight of HA (Chen et al. 1977). The E_2/E_3 value, which was used as the indicator of molecular size and weight of HA (Vidal et al. 2016), refers to the ratio of absorbances at 250 nm and 365 nm in the UV–Vis spectrum; the lower E_2/E_3 value, the larger molecular size of HA (Helms et al. 2008). The $\Delta \log K$ was viewed as the absorbances difference between 400 and 600 nm in the UV–Vis spectrum (Kumada 1987), studies had suggested that $\Delta \log K$ could be used to characterize the degree of the molecular condensation of HA; the lower $\Delta \log K$, the higher molecular condensation degree of HA (Giovanela et al. 2010). To better distinguish the specific influence of Ca^{2+} on molecular properties of three HA samples, we plotted the variations of E_2/E_3, E_4/E_6, and $\Delta \log K$ versus the total concentration of Ca^{2+} in the HA solutions in Fig. 2.

2.3.3 EEM fluorescence spectroscopy

The EEM fluorescence spectrum was often used to investigate the structure and composition of HA. In this study, we focused on changes of fluorescence signals in the EEM spectra along with the continuous adding of Ca^{2+}. Additionally, a series of fluorescence peaks of HA could be identified from the EEM spectrum (Senesi 1990; Coble 1996; Chen et al. 2003). The distribution of different types of fluorescence peaks as illustrated in Fig. 3 and summarized in Table 3. The fluorescence peaks in regions A and C are mainly related to carboxyl and carbonyl structures in natural organic matters (Wu and Tanoue 2001). The fluorescence peaks in region E are related to the SOM fraction with low molecular weight and high fluorescence effect (Wu et al. 2003). The fluorescence peaks in region B are related to two kinds of protein-like structures in natural organic matters (Wu et al. 2003). The EEM spectra of three HA samples at different total Ca^{2+} concentrations were shown in Fig. 4.

3 Results

3.1 Potentiometric titration

The potentiometric titration data of Ca^{2+} in three HA solutions (L1HA, L2HA, and L3HA) and their fit curves by Freundlich, Langmuir, Langmuir–Freundlich, and Toth models were plotted in Fig. 1 and fit parameters were listed in Table 4. It can be seen from Fig. 1 and Table 4 that the L3HA sample from the bottom layer of the limestone soil profile showed the lowest ability in taking Ca^{2+} from the solution, while the L2HA sample from the middle layer showed the highest ability. The results implied that adsorption most likely is the major mechanism that underlies the binding of Ca^{2+} and HA samples in the solutions since all three sets of titration data could be fit well by the classic Freundlich and Langmuir sorption models. Table 4 list the fit parameters of Freundlich, Langmuir, Langmuir–Freundlich, and Toth models. The K_F of the Freundlich model and Q_m of the other three models were closely related to sorption capacity, the fit K_F values showed an order of L2HA > L1HA > L3HA, the K_F of L2HA was about 18,320 while that of L3HA was about 2478, the fit Langmuir Q_m values showed the same trend of L2HA > L1HA > L3HA. In terms of the Langmuir–Freundlich model and the Toth model, they fit well for L3HA, acceptably for L2HA, and inferiorly for L1HA, indicating that these two models are not suitable to depict observations for all three HA samples. Moreover, the Tekim model failed completely (data not showed). All the same, the L3HA sample showed the lowest Q_m values of Langmuir–Freundlich and Toth models. The n value from the Freundlich model fitting was the lowest (0.475) for L3HA and the highest (0.865) for L2HA, which might suggest that the L3HA sample has the highest heterogeneous binding sites for Ca^{2+} while the L2HA sample has the lowest. The b value from the Langmuir model fitting was the highest (50.271) for L3HA, the lowest (6.242) for L2HA, and medium (15.407) for L1HA. The reverse variation trends of Q_m and b values among the three HA samples indicated that the intrinsic sorption mechanisms of Ca^{2+} on HA samples might be different from each other.

After the titration experiments, there were nonnegligible pH decrements in all three HA solutions, the pH of the solution decreased by 0.09, 0.10, and 0.07, respectively, for L1HA, L2HA, and L3HA. We believed these pH changes were significant and meaningful, because, on the one hand, these pH decrements should not derive from changes in the solution's ionic strength, which was controlled to be constant by 0.1 mol/L NaCl, and on the other hand, the high precise pH electrode of the titrator (Mettler Toledo T50) had an accuracy of $\pm$ 0.01, which is much smaller than observed pH decrements and such ensured that the measured pH decrements were not random errors. The pH decrements in titration experiments were consistent with Ca^{2+} sorption capacities in three HA samples, the higher is the sorption capacity the larger is the pH decrement, suggesting that Ca^{2+} ion may likely displace H^+ ion from the HA samples. This is consistent with the acidic functional group contents estimated from the ^{13}C-NMR spectra in

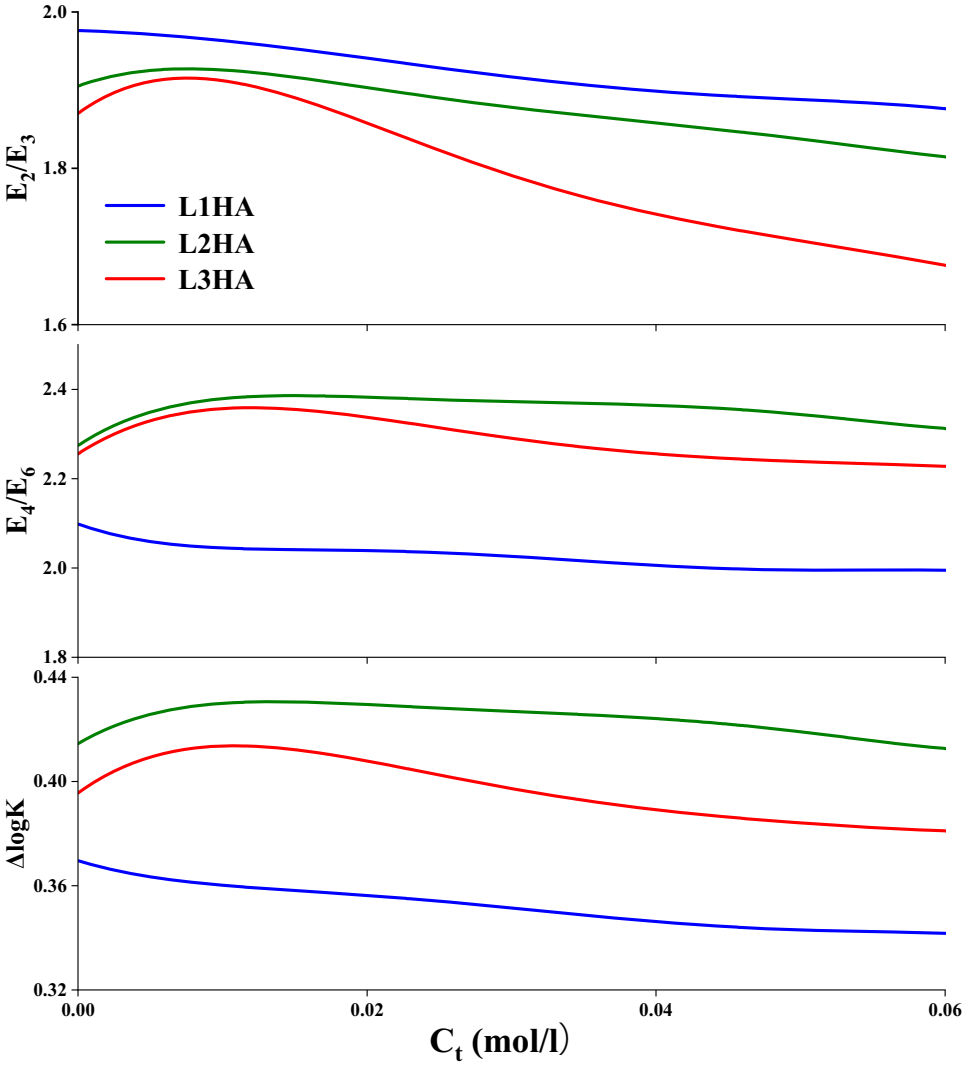

Fig. 2 The variations of E_2/E_3, E_4/E_6, and $\Delta \log K$ of three HA samples as the total concentration of Ca^{2+} increasing. *Note*: C_t (mol/L) is the total concentration of Ca^{2+} in the experiment system

three HA samples (Table 2) and the amounts of Ca^{2+} they have bound in the titration experiment. The pH changes verified that carboxyl and phenolic functional groups of HA are the main reaction sites for Ca^{2+}, where Ca^{2+} ion competes with H^+ ion and eventually replace H^+ to form Ca–HA complex. Therefore, we believed that the complex reaction is also crucial for the interaction of Ca^{2+} and HA.

3.2 UV–visible spectroscopy

The variations of UV–Vis spectra as increasing of the total Ca^{2+} content in HA solutions were numerically illustrated by plotting E_4/E_6, E_2/E_3, and $\Delta \log K$ versus the Ca^{2+} concentration in Fig. 2. The L1HA sample extracted from the upper layer of the limestone soil profile showed the least initial E_4/E_6 ratio among three HA samples and its E_4/E_6 ratio decreased continuously as the Ca^{2+} content in the solution was increased, implying that L1HA has the largest apparent molecular weight and becomes even bigger in the reaction with Ca^{2+}. The E_4/E_6 variations of L2HA and L3HA showed a similar pattern, their E_4/E_6 ratios increased as the increasing of the Ca^{2+} concentration in the low concentration range (< 0.010 mol/L) and then became decreasing when the concentration of Ca^{2+} was higher than 0.015 mol/L, indicating that different concentrations of Ca^{2+} may have different effects on the apparent molecular weight of L2HA and L3HA. The E_2/E_3 ratio and the $\Delta \log K$ value are also empirical proxies for complexity, condensation, aromaticity, and molecular size of SOM (Peuravuori and Pihlaja 1997; Giovanela et al. 2010; Enev et al. 2018). Generally, their values were decreased by the Ca^{2+} titration, implying that the apparent molecular structure of HA samples became more complex in the interaction with Ca^{2+}. However, their variation trends for three HA samples were not always consistent, indicating the multiplicity of their roles and the distinct characteristics of the HA samples.

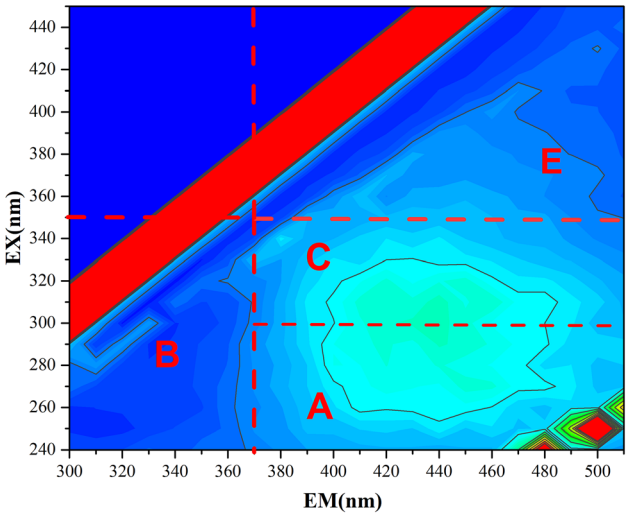

Fig. 3 The zone division of different types of fluorescence peak of the typical HA in the EEM spectrum. *Note*: **A** is the UV fulvic-like fluorescence peaks zone, **B** is the protein-like fluorescence peaks zone, **C** is the visible fulvic-like fluorescence peaks zone, **E** is the humic-like fluorescence peaks zone

Table 3 The zones of different types of fluorescence peaks in typical HA samples

Zone	EX (nm)	EM (nm)	Meaning
A	240–270	370–440	UV fulvic-like fluorescence peaks
B			
B1	260–290	300–320	Tyrosine-like fluorescence peaks
B2	260–290	320–350	Tryptophan-like fluorescence peaks
C	310–360	370–450	Visible fulvic-like fluorescence peaks
E	350–450	430–510	Humic-like fluorescence peaks

3.3 Fluorescence spectroscopy

The EEM spectra of three HA samples and their variations under different total Ca^{2+} concentrations were visibly different (Fig. 4). In general, the EEM spectra of all three HA samples shifted gradually but significantly when the concentration of Ca^{2+} increased from low to high, among them, the L2HA spectra showed the strongest peak intensity and the broadest peak area. It is visible in Fig. 4 that when the concentration of Ca^{2+} increased, the intensities of the humic-like fluorescence peaks (peak E) of all HA samples were abated, indicating that components of large molecular size and high fluorescence functional group content decreased when the concentration of Ca^{2+} increased. However, changes in the fulvic-like peaks (Peak A&C) and protein-like fluorescence peaks (Peak B) were barely distinguished. For better comparison, we picked out the peak intensity values from the four different zones, visible fulvic-like fluorescence peak zone (I, peak C), UV fulvic-like fluorescence peak zone (II, peak A), tryptophan-like fluorescence peak zone (III, peak B2) and tyrosine-like fluorescence peak zone (IV, peak B1) of EEM spectra (Fig. 4) and plotted them against the concentration of Ca^{2+} in Fig. 5. It can be seen that the intensity of the fulvic-like fluorescence peaks (I) decreased sharply when the total concentration of Ca^{2+} was below 0.01 mol/L, especially L2HA, then became relatively constant when the total concentration of Ca^{2+} was higher than 0.03 mol/L. The intensities of both visible fulvic-like fluorescence peaks (I) and UV fulvic-like fluorescence peaks (II) showed an order of L2HA > L1HA > L3HA, which is consistent with the trend of their total contents of carboxyl and phenolic groups (Table 2), again indicating that Ca^{2+} interacted mainly with carboxyl and phenolic groups of HA. The peak intensities of protein-like fluorescence peaks (III & IV) of all three HA samples increased as Ca^{2+} adding while L1HA showed the highest peak intensities. The protein-like structures of HA will not increase by adding Ca^{2+}, the increment of protein-like fluorescence peaks intensities most likely resulted from more exposure or aggregation of scattered protein-like structures in HA samples, implying the modification effects of Ca^{2+} on the structural configuration of HA samples in the solution.

4 Discussion

Studies on the karst rocky desertification in the southwest karst region of China had noticed that limestone soils in this region often have higher SOM contents than adjacent other soils (Wang et al. 2004; Ma et al. 2016). However, it was also often reported that the limestone soil region suffered more severe rocky desertification than adjacent regions of other soils when the overlying vegetation was spoiled (Zheng and Wang 2002; Di et al. 2019), which is quite disaccorded with the high SOM content in limestone soils since SOM is commonly considered as the binder of soil particles to resist soil erosion. Meanwhile, it was reported that SOM and metallic ions can form stable humic-metal complexes in soil (Lopez-Sangil and Rovira 2013; Bimüller et al. 2016). We speculated that the high calcium content in the limestone soil may play an essential role in the behaviors of limestone soils during the karst rocky desertification.

This study found that the combination of Ca^{2+} with HA molecules in the aqueous solution is a combination process of complexation and adsorption. The adsorption dominated the overall distribution of Ca^{2+} between solution and HA phases. This conclusion can be told by sorption model fittings results, where the two classic sorption models, Langmuir model, and Freundlich model, fit the titration

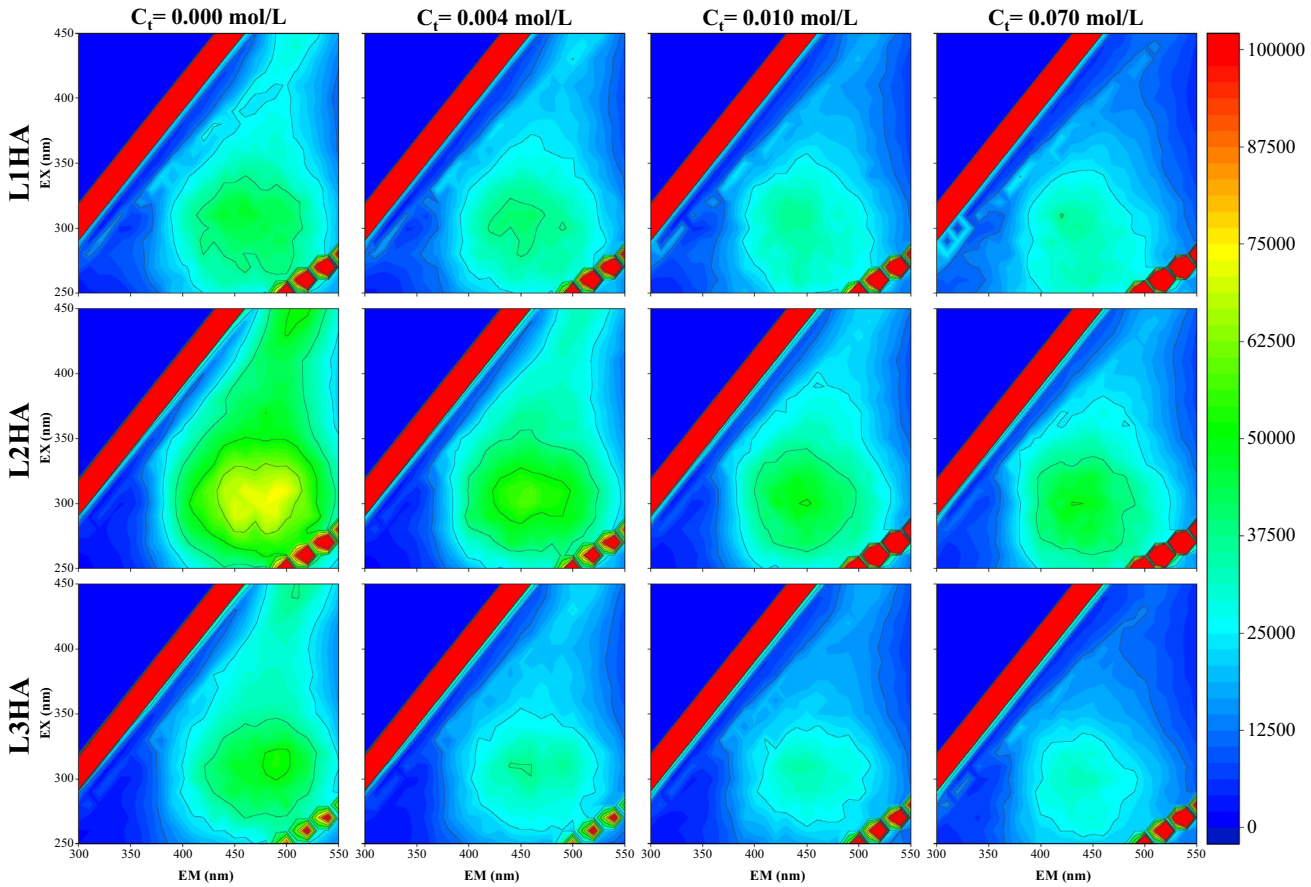

Fig. 4 The EEM fluorescence spectra of three HA samples at different total concentrations of Ca^{2+} in the experimental system. *Note*: C_t (mol/L) is the total concentration of Ca^{2+} in the experiment system

Table 4 The pH variations and the fitted isotherm parameters of different sorption models

Sample	Initial pH	End pH	Freundlich model			Langmuir model		
			n	K_F (mol/kg)/(mol/L)^n	R^2	Q_m (mol/L)	b (l/kg)	R^2
L1HA	*6.27*	*6.18*	0.701 ± 0.009	9403.785 ± 267.049	0.990	2615.535 ± 80.832	15.407 ± 0.745	0.988
L2HA	*6.26*	*6.16*	0.865 ± 0.005	18,320.248 ± 343.107	0.997	5656.350 ± 199.391	6.242 ± 0.266	0.998
L3HA	*6.30*	*6.23*	0.475 ± 0.011	2478.597 ± 96.581	0.960	813.706 ± 12.364	50.271 ± 1.978	0.979

	Langmuir–Freundlich model				Toth model			
	Q_m (mol/L)	b (L/mol)	n	R^2	Q_m (mol/L)	b (L/mol)	n	R^2
L1HA	7634.363 ± 3264.844	2.150 ± 1.615	0.777 ± 0.038	0.990	183,034.109 ± 500,333.016	0.808 ± 1.566	0.217 ± 0.107	0.990
L2HA	6560.741 ± 1063.354	5.020 ± 1.177	0.978 ± 0.022	0.998	5506.663 ± 1968.288	6.446 ± 2.122	1.000 ± 0.191	0.998
L3HA	832.663 ± 39.313	47.757 ± 5.189	0.973 ± 0.050	0.979	818.392 ± 55.397	50.371 ± 2.277	0.990 ± 0.115	0.978

data much better compared to Langmuir–Freundlich and Toth models, further the chemical sorption related Tekim model failed completely in fitting. It is reasonable to postulate that the main driving force for Ca^{2+} to combine with HA samples is the electrostatic attraction, hereby we believed that the combination of Ca–HA in limestone soils should not be as stable as the Ca–HA complexes mentioned in literatures (von Lützow et al. 2006; Liu 2009). The following real-time UV–Vis and EEM spectra showed that the combining with Ca^{2+} did modify the molecular configuration of HA, as shown in Fig. 2, the overall decreasing trends of E_2/E_3, E_4/E_6, and $\Delta \log K$ were found for all HA samples, indicating that when the concentration of Ca^{2+} in solution was high enough, the apparent molecular weight, size, and complexity of all HA samples in the solution increased uniformly, and, consequently, geochemical

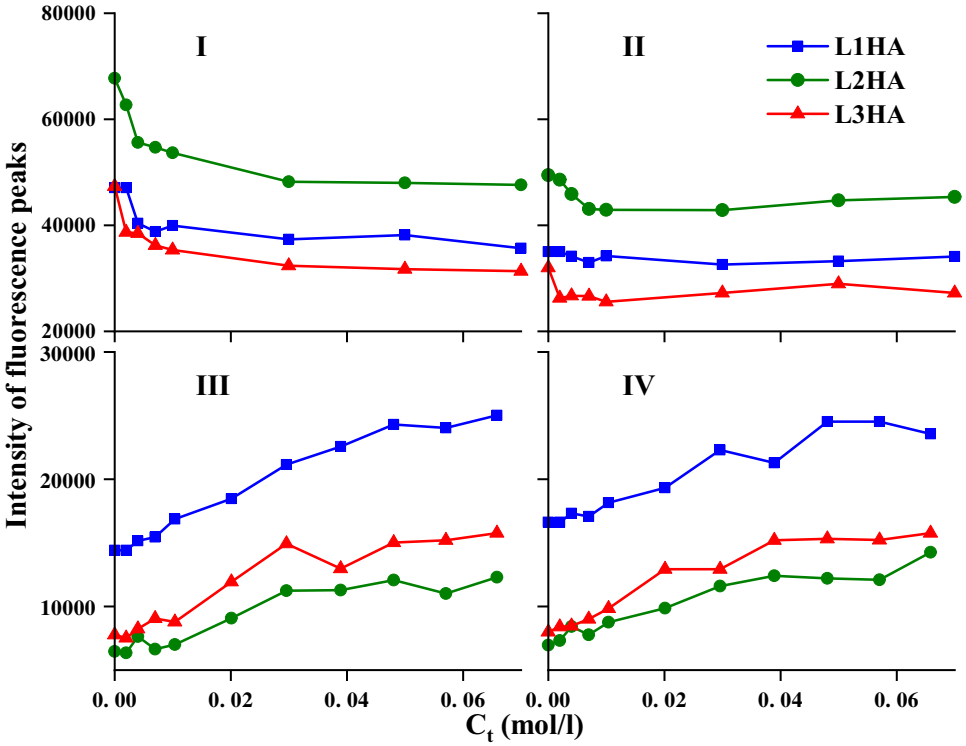

Fig. 5 The change of the fulvic-like and protein-like fluorescence peaks in HA samples with Ca^{2+} concentration increasing. *Note*: **I** stands for the change of the visible fulvic-like fluorescence peaks (peak C), **II** the change of the UV fulvic-like fluorescence peaks (peak A), **III** the change of the tryptophan-like fluorescence peaks (peak B2), **IV** the change of the tyrosine-like fluorescence peaks (peak B1)

behaviors of HA were different. Although the interaction of HA and Ca^{2+} found in this study was dominated by adsorption, complexation of HA and Ca^{2+} can be distinguished in the low concentration range of Ca^{2+} (< 0.01 mol/L), which is consistent with the prior report (Srivastava et al. 2006). This was supported by the variations of E_2/E_3, E_4/E_6, and $\Delta \log K$ showed in Fig. 2, their values increased (except L1HA) in the initial titration stage showing that the apparent molecular weight, size, and complexity of HA were reduced by complexing with Ca^{2+}. According to the Pearson theory (Pearson 1968), Ca^{2+} is a hard acid and oxygen-containing functional groups, such as carboxyl and phenolic functional groups, in HA are a series of the hard base, such Ca^{2+} should be bound well with carboxyl and phenolic functional groups in HA. The titration results showed that L2HA had the highest Ca-binding capacity, slightly higher than that of L1HA, and much higher than that of L3HA, and this trend is consistent with the contents of carboxyl and phenolic functional groups in three HA samples. Therefore, this study suggested that the carboxyl and phenolic functional groups in HA are the primary binding sites for Ca^{2+}. This conclusion was also supported by the observed pH decrements in the titration experiments and was consistent with prior conclusions that Ca^{2+} mainly interacts with carboxyl groups of HA (Peterson 1948; Leenheer et al. 1995). Nonetheless, the exact amount of Ca^{2+} complexed with HA cannot be estimated practically due to the indefinite buffer capacity of HA under experimental conditions of the present study.

Previous studies reported metal ions, such as Cu^{2+}, Pb^{2+}, Fe^{3+}, Fe^{2+} and Al^{3+}, complexed with HA and clay in soils forming inner-sphere or outer-sphere complexes (Peterson 1948; Senesi et al. 1992; Römer et al. 1998; Begum et al. 2018) or behaved as bridges to connect parted SOM fragments (Kloster et al. 2013) and by such retarded the degradation rate of SOM (Gerke 2010). Likewise, Ca^{2+} was proposed to bridge linking or flocculating small humic molecules and forming humic supramolecular structures in soils (Piccolo 2002), other studies suggested that Ca^{2+} could reduce the surface potential and electric field intensity of soil humic acids and lead to their aggregation and flocculation (Tian et al. 2020). The present study evaluated the interaction of Ca^{2+} and HA and investigated the effects of the Ca–HA combination to apparent molecular size, structure, and other physicochemical properties of three HA samples obtained from limestone soils of the southwest karst region of China. The results showed that the overall interactions of Ca^{2+} with three HA samples were predominated by adsorption, implying that the stability of the Ca–HA combination should be lower than that of those of Fe-HA and Al-HA, which is consistent with prior findings, HA formed inner sphere-type complexes with clay bridged by Fe^{3+} and Al^{3+} (Hemingway et al. 2019) but formed outer sphere-type complexes or humic supramolecules with clay bridged by Ca^{2+} (Kalbitz and Kaiser 2008). However, the distinctive difference between the titration curve of L3HA and those of L1HA and L2HA may suggest that binding reactions of Ca^{2+} to HA are related to acidic

functional group's distribution and the spatial configurations of HA.

The observed overall changes of E_2/E_3, E_4/E_6, $\Delta \log K$ values and EEM spectra of three HA samples indicated that the molecular space configuration of the HA samples became bigger and more complex and that some dispersive functional groups, like amino acid-like groups, were concentrated during the titration process. Furthermore, variations of these proxies (E_2/E_3, E_4/E_6, and $\Delta \log K$) at different concentration levels of Ca^{2+} for different HA samples were not always coincident, implying that manifold interaction mechanisms and properties of HA samples have comprehensive influences on the characteristics and behaviors of Ca–HA aggregates. Given Ca^{2+} is a relatively easily lost element of soil and whose content in the soil will decrease quickly in the long-term cultivation unless been complexed by SOM (Bubier et al. 2011; Meng et al. 2016; Moore et al. 2019), together with the finding of relatively low stability of HA-Ca could explain the common phenomenon in the southwest karst region of China that limestone soils with high TOC content degraded much faster than adjacent other soils when native vegetation covers were spoiled. When the limestone soil was exposed directly to the rain or runoff water erosion and the Ca^{2+} supplement from vegetation litters was stopped, Ca^{2+} in the humic-Ca structure would be washed out and humic materials once being protected by humic-Ca structure would become vulnerable to being washed away and many kinds of biochemical degradation.

5 Conclusion

The present study employed a joint experimental platform of a potentiometric titration, a UV–Vis spectroscopy, and a fluorescence spectroscopy and developed a sequential real-time monitoring method to investigate the interactions of Ca^{2+} and HA in the aqueous solution of the constant ion strength and the changes of apparent molecular characteristics of the HA samples in the interaction. The titration data indicated that the interaction of HA and Ca^{2+} was a combined process of complexation and adsorption in the experimental Ca^{2+} concentration range (up to 0.07 mol/L), and that adsorption was the dominated process, the overall distribution of Ca^{2+} between solution and HA fit well with classic adsorption models, Langmuir and Freundlich models, but not the chemical sorption related Temkin model. The complexation interaction of Ca^{2+} and HA could be distinguished only when the concentration of Ca^{2+} was low (less than 0.01 mol/L). The interaction of Ca^{2+} and HA showed remarkable influences on physicochemical properties of HA, the apparent molecular size, structure, and complexity of HA increased as more Ca^{2+} ions were bound, and such the refractory of HA to biochemical degradations and runoff erosions was increased. The high Ca^{2+} content is propitious to the SOM preservation in limestone soils and this could be accounted for the relatively high SOM content in limestone soils of the southwest karst region of China. However, the stability of the Ca–HA combination should be lower compared to complexes of HA with other bivalence metal ions, like Cu^{2+} and Pb^{2+}, therefore Ca^{2+} ion might be ready to dissociate from Ca–HA under strong erosions. In summary, we believed that the interaction of Ca^{2+} with SOM is vital to maintain the high SOM content in limestone soils of the study area, but the binding force of the Ca-SOM combination is not very strong, when the limestone soil received strong artificial disturbances, such as destroying of vegetation or cultivation, the combination of Ca and SOM will be spoiled by runoff water leaching and hence SOM in the limestone soil will become vulnerable to runoff erosions and biochemical degradations, eventually aggravate the karst rocky desertification. The present study investigated only the interaction of Ca^{2+} and HA, the comprehensive and systematic understandings of Ca^{2+} interacting with different SOM components in limestone soils are much needed to prevent karst rocky desertification and restore the ecological environment of karst rocky desertification sites.

Acknowledgements This research was supported by the National Natural Science Foundation of China (U1701241, U1612441, 41773147, and 41273149) and the Science Foundation of Guizhou (20113109).

References

Abate G, Masini JC (2001) Acid-basic and complexation properties of a sedimentary humic acid: a study on the Barra Bonita reservoir of Tietê river, São Paulo State, Brazil. J BrazChemSoc 12(1):109–116

Agnelli A, Celi L, Corti G (2002) The changes with depth of humic and fulvic acids extracted from the fine earth and rock fragments of a forest soil. Soil Sci 167(8):524–538

Aiken GR, Mcknight DM, Wershaw RL (1985) Humic substances in soil, sediment, and water: geochemistry, isolation and characterization. Soil Sci 142(5):323

Bai XY, Wang SJ, Xiong KN (2011) Assessing spatial-temporal evolution processes of karst rocky desertification land: indications for restoration strategies. Land Degrad Dev 24(1):47–56

Baldock JA, Skjemstad JO (2000) Role of the soil matrix and minerals in protecting natural organic materials against biological attack. Org Geochem 31(7):697–710

Begum ZA, Rahman IMM, Tate Y, Ichijo T, Hasegawa H (2018) Binding of proton and iron to lignite humic acid size-fractions in aqueous matrix. J Mol Liq 254:241–247

Bimüller C, Kreyling O, Kölbl A, von Lützow M, Kögel-Knabner I (2016) Carbon and nitrogen mineralization in hierarchically structured aggregates of different size. Soil Till Res 160:23–33

Bollag JM, Stotsky G (2000) Soil biochemistry. Marcel Dekker Inc., New York

Bubier JL, Smith R, Juutinen S, Moore TR, Minocha R, Long S, Minocha S (2011) Effects of nutrient addition on leaf chemistry, morphology, and photosynthetic capacity of three bog shrubs. Oecologia 167(2):355–368

Chen Y, Senesi N, Schnitzer M (1977) Information provided on humic substances by E_4/E_6 ratio. Soil Sci Soc Am J 41(2):352–358

Chen J, Gu B, Leboeuf EJ, Pan H, Dai S (2002) Spectroscopic characterization of the structural and functional properties of natural organic matter fractions. Chemosphere 48(1):59–68

Chen W, Westerhoff P, Leenheer JA, Booksh K (2003) Fluorescence excitation–emission matrix regional integration to quantify spectra for dissolved organic matter. Environ Sci Technol 37(24):5701–5710

Coble PG (1996) Characterization of marine and terrestrial DOM in seawater using excitation–emission matrix spectroscopy. Mar Chem 51(4):325–346

Coleman DC, Wall D (2014) Soil fauna: occurrence, biodiversity and roles in ecosystem function. In: Paul EA (ed) Soil microbiology, ecology and biochemistry, 4th edn. Academic Press, San Diego

Derek F, Paul W (2007) Karst hydrogeology and geomorphology. Wiley, London

Di XY, Xiao BH, Dong H, Wang SJ (2019) Implication of different humic acid fractions in soils under karst rocky desertification. Catena 174:308–315

Duchaufour P (1976) Dynamics of organic matter in soils of temperate regions: its action on pedogenesis. Geoderma 15(1):31–40

Enev V, Pospisilova L, Klučáková M, Liptaj T, Doskočil L (2018) Spectral characterization of selected humic substances. Soil Water Res 9(1):9–17

Gerke J (2010) Aluminium and iron(III) species in the soil solution including organic complexes with citrate and humic substances. J Plant Nutr Soil Sci 160(3):427–432

Giovanela M, Crespo JS, Antunes M, Adamatti DS, Fernandes AN, Barison A, Silva C, Guégan R, Motelica-Heino M, Sierra M (2010) Chemical and spectroscopic characterization of humic acids extracted from the bottom sediments of a Brazilian subtropical microbasin. J Mol Struct 981(1–3):111–119

Grünewald G, Kaiser K, Jahn R, Guggenberger G (2006) Organic matter stabilization in young calcareous soils as revealed by density fractionation and analysis of lignin-derived constituents. Org Geochem 37(11):1573–1589

He W, Chen M, Park JE, Hur J (2016) Molecular diversity of riverine alkaline-extractable sediment organic matter and its linkages with spectral indicators and molecular size distributions. Water Res 100:222–231

Helms JR, Stubbins A, Ritchie JD, Minor EC, Kieber DJ, Mopper K (2008) Absorption spectral slopes and slope ratios as indicators of molecular weight, source, and photobleaching of chromophoric dissolved organic matter. Limnol Oceanogr 53(3):955–969

Hemingway JD, Rothman DH, Grant KE, Rosengard SZ, Eglinton TI, Derry LA, Galy VV (2019) Mineral protection regulates long-term global preservation of natural organic carbon. Nature 570(7760):228–231

Janoš P, Krizenecka S, Madronova L (2008) Acid-base titration curves of solid humic acids. React Funct Polym 68(1):242–247

Jin J, Zimmerman AR (2010) Abiotic interactions of natural dissolved organic matter and carbonate aquifer rock. Appl Geochem 25(3):472–484

Jin P, Song J, Yang L, Jin X, Wang XC (2018) Selective binding behavior of humic acid removal by aluminum coagulation. Environ Pollut 233:290–298

Jones MN, Bryan ND (1998) Colloidal properties of humic substance. Adv Colloid Interface Sci 78(1):1–48

Kalbitz K, Kaiser K (2008) Contribution of dissolved organic matter to carbon storage in forest mineral soils. J Plant Nutr Soil Sci 171(1):52–60

Kloster N, Brigante M, Zanini G, Avena M (2013) Aggregation kinetics of humic acids in the presence of calcium ions. Colloids Surf A 427(24):76–82

Kogelknabner I, Guggenberger G, Kleber M, Kandeler E, Kalbitz K, Scheu S, Eusterhues K, Leinweber P (2008) Organo-mineral associations in temperate soils: integrating biology, mineralogy and organic matter chemistry. J Plant Nutr Soil Sci 171(1):61–82

Kumada K (1987) Chemistry of soil organic matter. Japan Scientific Societies Press, Amsterdam

Leenheer JA, Brown GK, MacCarthy P, Cabaniss SE (1995) Models of metal binding structures in fulvic acid from the Suwannee River, Georgia. Environ Sci Technol 29(2):399–405

Lehmann J, Kleber M (2015) The contentious nature of soil organic matter. Nature 528(7580):60–68

Liu CQ (2009) Biogeochemical processes and cycling of the nutrients in the earth's surface—nutrient cycling in soil and plant system in karstic catchment. Science Press, Beijing

Lopez-Sangil L, Rovira P (2013) Sequential chemical extractions of the mineral-associated soil organic matter: an integrated approach for the fractionation of organo-mineral complexes. Soil Biol Biochem 62(5):57–67

Ma LG, Xiao BH, Huang WL, Wang SJ (2016) Characteristics and distributions of humic acids in two soil profiles of the southwest China Karst area. Acta Geochimica 35(1):85–94

Meng W, Larmola T, Murphy MT, Moore TR, Bubier JL (2016) Stoichiometric response of shrubs and mosses to long-term nutrient (N, P and K) addition in an ombrotrophic peatland. Plant Soil 400:403–416

Moore TR, Knorr KH, Thompson L, Roy C, Bubier JL (2019) The effect of long-term fertilization on peat in an ombrotrophic bog. Geoderma 343:176–186

Oades JM (1988) The retention of organic matter in soils. Biogeochemistry 5(1):35–70

Osman KT (2013) Soil organic matter. Soils: principles, properties and management. Springer, Dordrecht, pp 89–96

Pearson RG (1968) Hard and soft acids and bases, HSAB, part 1: fundamental principles. J ChemEduc 45(9):581–587

Peterson JB (1948) Calcium linkage, a mechanism in soil granulation. Soil Sci Soc Am J 12(C):29

Peuravuori J, Pihlaja K (1997) Molecular size distribution and spectroscopic properties of aquatic humic substances. Anal Chim Acta 337:17

Piccolo A (2002) The supramolecular structure of humic substances: a novel understanding of humus chemistry and implications in soil science. Adv Agron 75(02):57–134

Piccolo A, Mbagwu JSC (1994) Humic substances and surfactants effects on the stability of two tropical soils. Soil Sci Soc Am J 58(58):950–955

Plank J, Bassioni G (2007) Adsorption of carboxylate anions on a $CaCO_3$ surface. Z Naturforsch B 62(10):1277–1284

Römer W, Patzke R, Gerke J (1998) Die Kupferaufnahme von Rotklee und Weidelgrasaus Cu-Nitrat-, Huminstoff-Cu- und Cu-Citrat-Lösungen. In: Merbach W (ed) Pflanzenernährung, Wurzelleistung und Exsudation. Vieweg+Teubner Verlag, Wiesbaden (in German)

Schmidt MWI, Torn MS, Abiven S, Dittmar T, Guggenberger G, Janssens IA, Kleber M, Kogel-Knabner I, Lehmann J, Manning DAC, Nannipieri P, Rasse DP, Weiner S, Trumbore SE (2011) Persistence of soil organic matter as an ecosystem property. Nature 478(7367):49–56

Senesi N (1990) Molecular and quantitative aspects of the chemistry of fulvic acid and its interactions with metal ions and organic

chemicals: part I. The electron spin resonance approach. Anal Chim Acta 232(3):51–75
Senesi N, Saiz-Jiminez C, Miano TM (1992) Spectroscopic characterization of metal-humic acid-like complexes of earthworm-composted organic wastes. Sci Total Environ 117–118:111–120
Sollins P, Homan P, Caldwell BA (1996) Stabilization and destabilization of soil organic matter: mechanisms and controls. Geoderma 74(1–2):65–105
Srivastava VC, Mall ID, Mishra IM (2006) Equilibrium modelling of single and binary adsorption of cadmium and nickel onto bagasse fly ash. Chem Eng J 117(1):79–91
Stevenson FJ (1994) Humus chemistry. Genesis, composition, reactions. Wiley, New York
Tian T, Liu Z, Zhu F, Hartley W, Ye Y, Xue S (2020) Improvement of aggregate-associated organic carbon and its stability in bauxite residue by substrate amendment addition. Land Degrad Dev 31:2405–2416
Vidal FJR, Schlenger P, García-Valverde M (2016) Monitoring changes in the structure and properties of humic substances following ozonation using UV–Vis, FTIR and ^{1}H NMR techniques. Sci Total Environ 541:623–637
von Lützow M, Kogel-Knabner I, Ekschmitt K, Matzner E, Guggenberger G, Marschner B, Flessa H (2006) Stabilization of organic matter in temperate soils: mechanisms and their relevance under different soil conditions—a review. Eur J Soil Sci 57(4):426–445
Wang SJ (2003) The most serious eco-geologically environmental problem in southwestern China—karst rocky desertification. Bull Mineral Petrol Geochem 22(2):120–126
Wang SJ, Liu QM, Zhang DF (2004) Karst rocky desertification in southwestern China: geomorphology, landuse, impact and rehabilitation. Land Degrad Dev 15(2):115–121
Wu FC, Tanoue E (2001) Isolation and partial characterization of dissolved copper-complexing ligands in streamwaters. Environ Sci Technol 35(18):3646–3652
Wu FC, Tanoue E, Liu CQ (2003) Fluorescence and amino acid characteristics of molecular size fractions of DOM in the waters of Lake Biwa. Biogeochemistry 65(2):245–257
Yan Y, Dai Q, Jin L, Wang X (2019) Geometric morphology and soil properties of shallow karst fissures in an area of karst rocky desertification in SW China. Catena 174:48–58
Zhao J, Chen S, Hu R, Li Y (2017) Aggregate stability and size distribution of red soils under different land uses integrally regulated by soil organic matter, and iron and aluminum oxides. Soil Till Res 167:73–79
Zheng YC, Wang SJ (2002) Geological cause of calcareous soil erosion and land rocky desertification in karst area, Guizhou province. Resour Environ Yangtza Basin 11:461–465